Journal of Luminescence 247 (2022) 118860

Contents lists available at ScienceDirect

Journal of Luminescence

journal homepage: www.elsevier.com/locate/jlumin

Optical properties of hydrothermally deposited Ni and Co doped nanostructured ZnO thin films as scintillating coatings for beta-particles detection

Eugene Chubenko [a,*], Mohsin Wahioh Alhamd [a,b], Vitaly Bondarenko [a]

[a] Belarusian State University of Informatics and Radioelectronics, 220013, P. Brovka str. 6, Minsk, Belarus
[b] Atomic Energy Commission, Directorate of Research and Development, 765, Baghdad, Iraq

ARTICLE INFO

Keywords:
Zinc oxide
Hydrothermal deposition
Photoluminescence
Cathodoluminescence
X-ray diffractometry
Raman spectroscopy

ABSTRACT

The optical properties of ZnO films doped with the Ni and Co transition metals that were hydrothermally deposited on a silicon substrate are discussed. The SEM, EDX, XRD and Raman spectroscopy studies showed that the films deposited have a compact crystalline structure and can be considered as nanostructured polycrystalline ZnO films doped with Ni and Co and designated as ZnO:Ni and ZnO:Co, respectively. Under optical and electronic excitation, the films demonstrated both near-band-edge ultraviolet and visible range luminescence due to crystal lattice defects. The highest intensity of the ultraviolet luminescence with a fast decay was achieved for the ZnO:Ni and ZnO:Co samples deposited in the 0.05 M solutions of Ni or Co nitrate salts. Wide luminescence spectra make the films obtained promising as luminophore or scintillating coatings for the beta-particles detection including structures integrated with silicon circuits, for example, solid state silicon-based radiation counters.

1. Introduction

Zinc oxide (ZnO) is a well-known direct wide band-gap semiconductor used in various optoelectronic and optical devices such as light-emitting diodes, lasers, luminescent coatings and scintillators [1–3]. The 3.37 eV band gap at the room temperature indicates that ZnO should exhibit a luminescence in the ultraviolet (UV) range, and it does exhibit the intense near-band-edge (NBE) emission of the exciton nature [1,4]. The high efficiency of this process is due to the high exciton binding energy of 60 meV [1,4,5]. In addition to the exciton luminescence, ZnO also exhibits emission in the visible range. This band known as "green luminescence" is due to crystal lattice defects, particularly oxygen vacancies and interstitials as well as various uncontrolled and intentionally implanted impurities [4,6].

Scintillator materials should meet a number of specific requirements, such as a high light output, fast response, high density, chemical, mechanical and radiation stability, and low cost [7,8]. There is no universal material to cover all of them. Nowadays both inorganic and organic scintillators are used for various applications [8,9]. Organic scintillators usually based on a polymer matrix filled with organic luminophore have high performance but low radiation stopping power because they consist only from lightweight non-metal elements with low element number Z [9]. Inorganic materials include heavier metal elements and have greater radiation stopping power but longer luminescence decay [8].

ZnO long ago was proposed as inorganic semiconductor scintillator material. However, low stopping power for high energy gamma as well as difficulties in obtaining single crystals make it not very suitable for this task [4,10]. In few last decades it was discovered that even in the polycrystalline or powder form it has very good detecting capability for X-ray quanta, alpha and beta particles [10–13]. Pure intrinsic *i*-ZnO rarely used as scintillating coatings or glasses. Usually ZnO is doped with different metal impurities. The most popular are gallium, indium, magnesium, lithium and zinc [7,10–14]. Most of the listed elements play role of shallow donors in the ZnO band structure and can stabilize optical properties and improve its characteristics [3]. Their presence leads only to a slight modification of the ZnO crystal lattice structure and a change in the material band gap [3,14,15]. Gallium doping considered as the best choice to create ZnO-based scintillating films and materials [15]. However, some other less expensive metals can also be used for such purpose. For example, ZnO doping with transition metals of moderate Z (Ni or Co) leads to the stabilization of its characteristics and the luminescence enhancement [16,17].

* Corresponding author.
E-mail address: eugene.chubenko@gmail.com (E. Chubenko).

https://doi.org/10.1016/j.jlumin.2022.118860
Received 30 June 2021; Received in revised form 7 March 2022; Accepted 24 March 2022
Available online 2 April 2022

In this paper the photo- and cathodoluminescence of Ni and Co-doped ZnO thin films obtained by the hydrothermal method on silicon wafers coated with a thin atomic-layer-deposited (ALD) *i*-ZnO sublayer is discussed.

2. Experimental

Highly doped n^+ (100) monocrystalline silicon (Si) wafers covered with a 100-nm SiO_2 layer and a 30-nm ALD-deposited intrinsic *i*-ZnO sublayer were used for the ZnO deposition. The hydrothermal ZnO deposition was carried out in the aqueous equimolar 0.1 M zinc nitrate ($Zn(NO_3)_2$) and hexamethylenetetramine (HMTA) solution based on deionized water (~17 Ω × cm). Ni or Co nitrates ($Ni(NO_3)_2$ and $Co(NO_3)_2$) in various concentrations from 0.025 to 0.1 M were added to the solution as precursors to dope ZnO with corresponding metal. All chemicals used were of the analytical grade. The pH of the solution was normalized to 5.2 at room temperature by adding few drops of concentrated nitric acid (HNO_3). Prepared substrates were cleaned in deionized water, placed front side down in a thermostatically controlledglass autoclave and held at 85 °C for 2 h. Then substrates were extracted from the hot solution, cleaned in deionized water and dried in a warm air flow.

The morphology of the ZnO films obtained was studied with a Hitachi S-4800 scanning electron microscope (SEM). Energy-dispersive X-ray spectroscopy microanalysis (EDX) was carried out with a Bruker QUANTAX 200 analyzer. A DRON-3M X-ray diffractometer was used for XRD analysis. Raman spectra were studied with a SOL Instruments 3D scanning laser confocal Raman microscope Confotec NR500, wavelength of 473 nm was used for the excitation at that. Photoluminescence (PL) spectra were registered with a spectroscopic complex based on a Solar TII MS 7504i monochromator-spectrograph equipped with a CCD camera. PL of the ZnO was excited with monochromatic 345-nm light. All optical measurements were carried out at room temperature. To simulate the beta-particle irradiation behavior of the samples obtained, the cathodoluminescence (CL) was measured on a MDR-23 computerized spectrograph equipped with a photomultiplier tube as a detector, using a 2 keV electron beam and low current (<1 nA) to minimize sample heating. The electrical conductivity of the samples was measured by a standard four probe method using a Metrohm Autolab PGStat 302 N potentiostat/galvanostat as a power source. Sharpened copper probes in a linear configuration were used to contact deposited film.

3. Results

According to the SEM study, the films obtained consist of closely packed crystallites (Fig. 1). Surface plane view images revealed the hexagonal shape of the crystallites which is inherent to ZnO with hexagonal wurtzite crystal lattice, the most stable modification of ZnO [2,4]. The average size of the crystallites is about 100–300 μm. The thickness of obtained films was almost the same for different concentration of Ni^{2+} and Co^{2+} ions in the range from 0.025 to 0.1 M. For Ni-doped samples, it was about 1 μm, and for Co-doped ZnO films, it was close to 2 μm. According to EDX analysis, the concentration of Ni atoms in the sample obtained in the 0.025 M $Ni(NO_3)_2$ solution is 0.04 at.%. This corresponds to the doping level of ~$2{\cdot}10^{19}$ cm^{-3}. For ZnO films deposited from 0.05 to 0.1 M solutions of $Ni(NO_3)_2$, the Ni concentration is 0.1 and 1.1 at.%, corresponding to $5{\cdot}10^{19}$ cm^{-3} and $5.5{\cdot}10^{20}$ cm^{-3}, respectively. The concentration of Co atoms in the obtained films regardless the initial Co^{2+} concentration in the solution was below the detection limit and hence below. The concentration ratio of Zn/O atoms was close to unity, indicating that the obtained ZnO films were almost stoichiometric [1,2,4]. The measured resistivity of the films decreases from 0.73 Ω × cm for undoped ZnO to 2.5 … 6 × 10^{-2} Ω × cm for the samples corresponding to 0.1 M transition metal ion concentration in the deposition solution.

According to the results of the XRD study (Fig. 2), the samples

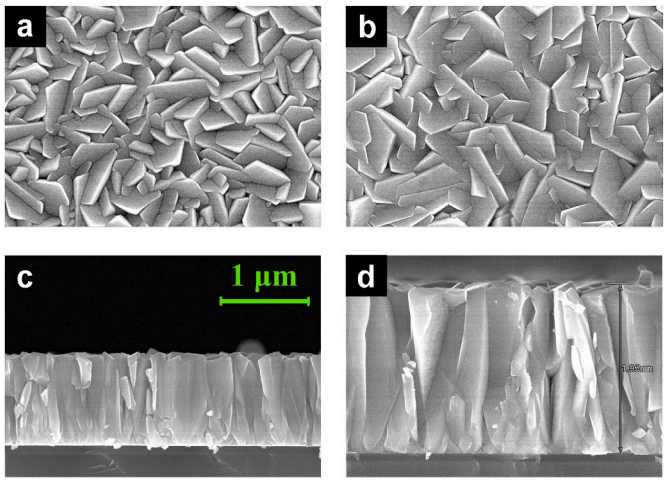

Fig. 1. SEM images of the surface and cross-section of the samples obtained from the $Zn(NO_3)_2$ solution containing either 0,025 M $Ni(NO_3)_2$ (a, c) or 0,025 M $Co(NO_3)_2$ (b, d). 1 μm scalebar is common for all images.

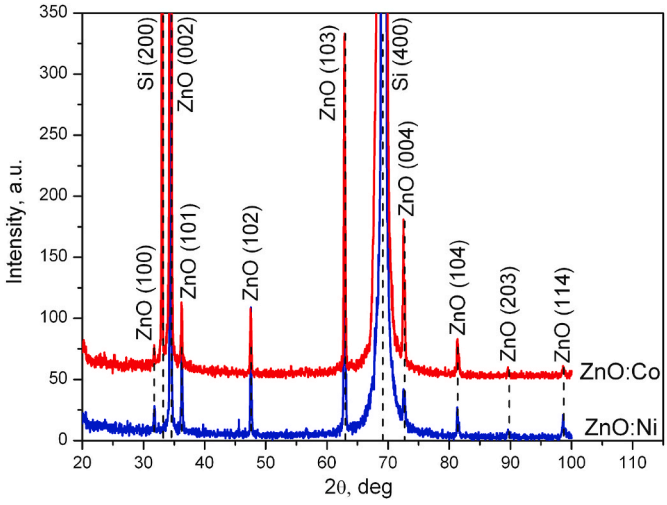

Fig. 2. XRD spectra of the samples obtained from $Zn(NO_3)_2$ solution containing either 0,025 M $Ni(NO_3)_2$ or 0,025 M $Co(NO_3)_2$. The peaks are identified using the ICDD database.

demonstrate multiple peaks corresponding to different phases. Strong peaks at 2θ = 32.9° and 69.3° correspond to the forbidden (200) and common (400) reflections of the monocrystalline silicon substrate crystal planes [18]. The clearly visible peaks at 2θ = 34.43°, 36.27°, 47.55°, 62.87° and 72.51° correspond to reflections from (002), (101), (102), (130) and (004) ZnO crystal planes. Some less intensive ZnO-related peaks are also presented on the XRD pattern: at 31.75°, 81.31°, and 98.63°. They correspond to (100), (203) and (114) planes. Large number of the sharp ZnO peaks visible on the XRD spectra defines the films obtained as structured polycrystalline with the dominant direction (002).

The Raman spectra for both Ni and Co containing ZnO films (Fig. 3a and b) are dominated by the first order Si threefold degenerate optical phonon mode (LO+2TO) with a maximum at 521.2 cm^{-1} and the second order peak (2TO) at 940–985 cm^{-1} [19]. Also, the Si transversal acoustic (2 TA) mode at around 300 cm^{-1} is presented [19].

ZnO has several optically active vibration modes visible on Raman spectra [4]. The obtained samples with small amount of Ni and Co dopant atoms (see spectra labeled as "0.025 M" on Fig. 3, *a* and *b*) demonstrate first order bands at around 437 and 575 cm^{-1}

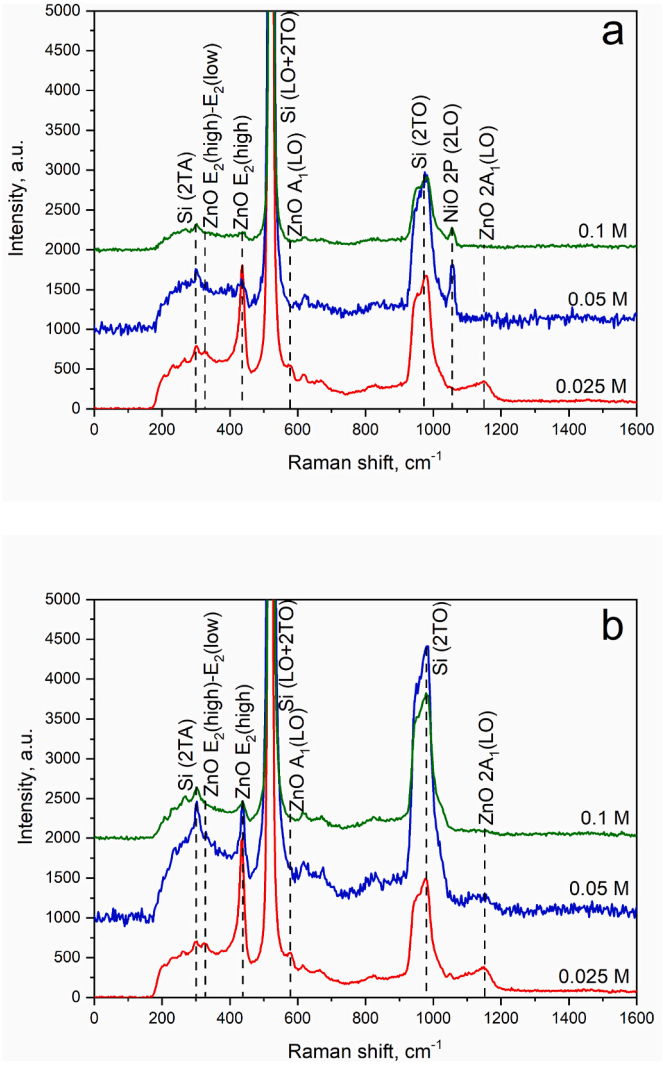

Fig. 3. Raman spectra of the samples obtained in the $Zn(NO_3)_2$ solution containing $Ni(NO_3)_2$ (a) and $Co(NO_3)_2$ (b) of different concentrations.

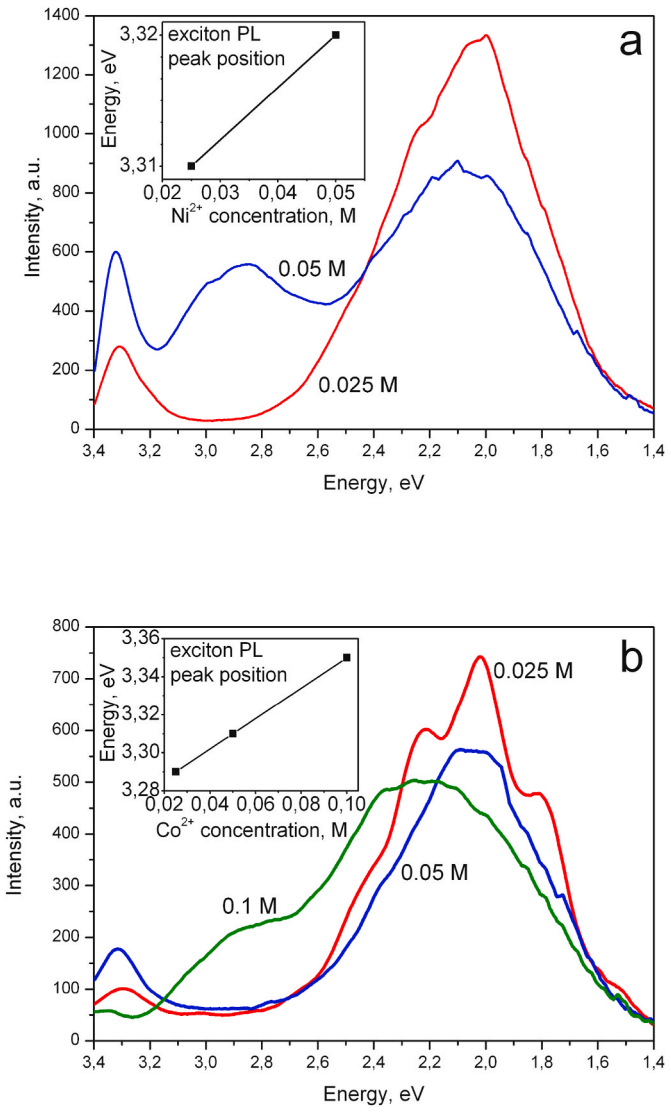

Fig. 4. Room temperature PL spectra of the samples obtained from $Zn(NO_3)_2$ solution containing $Ni(NO_3)_2$ (a) and $Co(NO_3)_2$ (b) of different concentration. Inserts show the exciton PL peak position for different dopants concentration in the solution.

corresponding to ZnO non-polar E_2(high) and longitudinal-optical A_1(LO) branches, second order $2A_1$(LO) at 1146 cm^{-1} and combinational E_2(high)-E_2(low) bands at 326 cm^{-1} [4,20,21]. The intensity of the ZnO Raman bands decreases as a dopant metal concentration in the film increases. The position of the band corresponding to the E_2(high) branch shifts to higher wavenumbers with increasing the concentration of dopant atoms from 437 to 440 cm^{-1} for Ni-containing ZnO films and from 437 to 439 cm^{-1} for Co-containing samples. Ni containing coatings with the dopant concentration above 0.05 M also possess a band related to the nickel oxide (NiO) 2LO vibration mode with maximum at 1048 cm^{-1} [22,23]. This band is not presented in the Co-containing films.

PL measurements of the ZnO coatings containing Ni atoms (Fig. 4, *a*) revealed three distinguishable bands on the spectra corresponding to different irradiation recombination processes.

The PL band in the UV range with a maximum at 3.31 eV is the NBE band corresponding to the recombination of bound excitons and the number of shallow donor-acceptor irradiative processes [4]. It has an asymmetrical "tail" in the low energy range defined by the number of phonon replicas [4]. They could not be resolved at room temperature. The maximum of NBE band shifts to higher energy from 3.31 to 3.32 eV as the concentration of Ni cations in the deposition solution increases. Its intensity increases more than twofold for the sample made in the solution with a higher concentration of Ni^{2+} ions (0.05 M). However, for the sample obtained in the 0.1 M $Ni(NO_3)_2$ solution, the PL spectra including NBE band are totally quenched.

The high intensity band with a maximum at 2.03–2.07 eV corresponds to oxygen related ZnO crystal lattice defects, namely oxygen vacancies V_O and oxygen interstitial atoms O_i [4,24,25]. The energy of the irradiative carrier recombination from the shallow donor levels of interstitial zinc atoms Zn_i to the oxygen vacancy V_O level is 2.24 eV and to the oxygen interstitial atom level O_i is 2.06 eV (see schematic ZnO band diagram at Fig. 5). The observed band has a prominent asymmetry, indicating that both processes are responsible for its appearance. The maximum position of that band shifts to higher energy with increasing the Ni concentration in the deposition solution. Thus, the recombination via V_O levels becomes more probable than through O_i levels, *i.e.* the concentration of interstitial oxygen atoms decreases. At the Ni concentration of 0.05 M, an additional PL band with a maximum at 2.85 eV appears. The energy of this band corresponds to transitions from the interstitial zinc atoms levels to the levels of zinc vacancy $Zn_i \rightarrow V_{Zn}$ (Fig. 5) [24,25].

The photoluminescence of Co-doped ZnO coatings shows a similar behavior. The NBE luminescence band maximum shifts from 3.29 to 3.35 eV when the concentration of cobalt in the deposition solution is

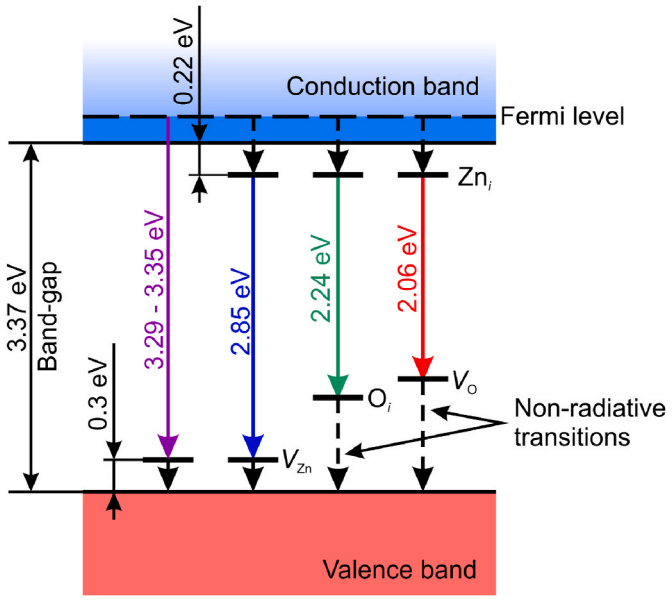

Fig. 5. Schematic energy band structure for degenerative doped *n*-type ZnO.

increased from 0.025 to 0.1 M. NBE luminescence intensity becomes higher for the sample obtained in the 0.05 M solution but then decreases with the increase of the Co concentration. The oxygen defect luminescence band maximum also shifts to higher energy with the Co concentration and at the same time its intensity slightly decreases. A noticeable interference was observed in the luminescence spectra of the sample obtained in the 0.025 M solution. At the high Co concentration of 0.1 M, a new band with a maximum at 2.85 eV corresponding to $Zn_i \rightarrow V_{Zn}$ transitions also appears. The incorporation of Co^{2+} ions into the ZnO crystal lattice may also develop a blue PL band, however its efficiency is very low compared to the intensity of the NBE and defect-related bands [26]. The CL spectra of the samples obtained in the solution containing 0.05 M Ni and Co are presented in Fig. 6. The samples showed the NBE luminescence band with a maximum at 3.31–3.32 eV and the band associated with oxygen defects with a maximum at 2.15–2.17 eV. The Ni-doped ZnO film also demonstrated the luminescence band in the blue range with a maximum at 2.86 eV corresponding to the $Zn_i \rightarrow V_{Zn}$ transitions.

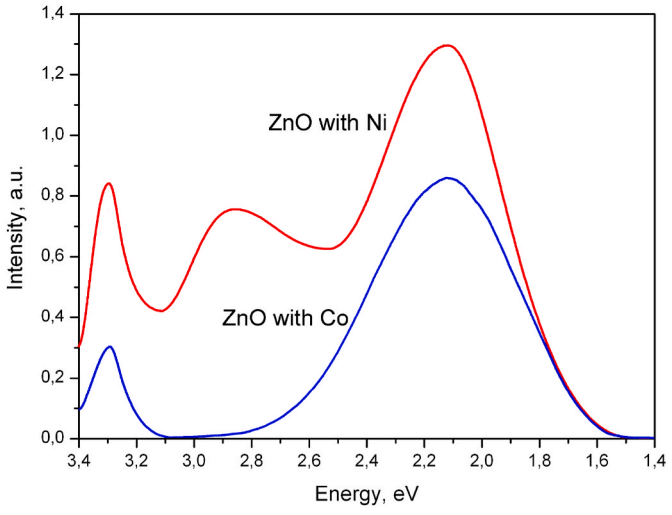

Fig. 6. CL spectra of the samples obtained from $Zn(NO_3)_2$ solution containing 0.05 M $Ni(NO_3)_2$ and $Co(NO_3)_2$.

4. Discussion

According to the SEM and XRD studies, the films obtained consist of ZnO crystallites with a hexagonal wurtzite crystal lattice tightly packed in a nanostructured polycrystalline film. In the case of the Ni doping, the dopant concentration increases with the increase of its concentration in the deposition solution. The Co concentration remains below the sensitivity of the EDX method used. However, considering the results of the PL study, Co atoms are certainly presented in the ZnO film and affect the recombination processes in the same way as Ni atoms do.

Raman and XRD studies showed the presence of crystalline ZnO phase and did not reveal the presence of Co oxide or hydroxide phases. However, when the Ni concentration in the deposition solution is high (above 0.05 M), the NiO band appears in the Raman spectra. Ni is known to have a low solubility in ZnO, which do not exceed 2.5 at.% at the synthesis temperature of 358 K [26]. However, even the Ni concentration of 0.1–1.1 at.% in the obtained ZnO film was sufficient for the appearance of local clusters where the Ni concentration exceeded its solubility and the formation of the NiO phase occurred. The Co solubility in ZnO is high and can reach 26 at.% at 358 K [27] and the formation of CoO was not expected. Also, the ZnO E_2(high) band shifted to higher wavenumbers with increasing the concentration of Ni and Co atoms in the deposition solution. That indicates the increase of the ZnO crystal lattice disorder caused of the incorporation of transition metal atoms [28,29]. Thus the films obtained can be considered as doped with Ni and Co and hereinafter will be referred as ZnO:Ni and ZnO:Co. Higher Ni atoms involvement into ZnO precipitation and grows process leads not only to higher concentration of transition metal in the resulting structure compared to Co doping, but also affect the deposition rate. Therefore, the thickness of the ZnO:Ni film is half that of the ZnO:Co coating.

The analysis of the PL and CL of the samples obtained revealed several atypical features for ZnO:Ni and ZnO:Co. Numerical calculations and experimental data have shown that the doping with Ni in high concentrations leads to a significant narrowing of the ZnO optical band [30,31], despite the fact that NiO has a band-gap of approximately 3.6–4.2 eV [32,33] and this value is higher than the ZnO bandgap width (3.37 eV at 300 K). According to the Vegard's law [34], the $Zn_{1-x}Ni_xO$ ternary composition should have an intermediate band-gap energy value between intrinsic ZnO and NiO [3] but this is not the case. The introduction of Ni inside the ZnO crystal structure leads to the formation of electron occupied Ni 3*d* states which mix strongly with the oxygen O 2*p* states in the valence band, shifting its maximum upwards in energy and narrowing the ZnO band-gap from the bottom [30]. At the same time the conduction band minimum also decreases in energy, further narrowing the ZnO:Ni band-gap [30].

However, the results of our experiments showed that the irradiative recombination energy in the UV region increases slightly with the increase in the concentration of Ni and Co transition metals. It is known that they serve as donors in semiconductor ZnO [16,17] and at the achieved levels of Ni and Co concentrations resulting ZnO:Ni and ZnO:Co can be considered as degenerate semiconductors. At high concentrations of doping atoms in *n*-type degenerate semiconductors, the Moss-Burstein effect takes place [16,35]. When the Fermi level rises above the bottom of the conduction band, all permitted states below it are occupied by carriers. In this condition, the excitation and recombination energy of electron-hole pairs $h\nu$ become the sum of the band-gap energy E_g and the Moss-Burstein blue-shift energy ΔE_{BM} minus the energy shift caused by the renormalization effect of bands ΔE_{Rn}: $h\nu = E_g + \Delta E_{BM} - \Delta E_{Rn}$ [35,36]. A more remarkable effect is the growth of the UV luminescence efficiency with increasing concentration of doping atoms in the ZnO:Ni and ZnO:Co films obtained. At the room temperature, the dominant luminescence mechanism in the UV range in doped or defect ZnO is not the neutral donor or acceptor bound exciton emission (D^0X or A^0X) [3,4,37] but the free-electron/neutral acceptor irradiative recombination (eA^0) [35,36]. The efficiency of this process increases with the carrier concentration in the conduction band [38]. The decrease in the

resistivity of the obtained films with the increase in the dopant concentration confirms that the described process may be responsible for the observed luminescence behavior. The NBE luminescence band in ZnO has a fast decay [4,39] and increasing its intensity compared to the defect band is important to obtain an effective scintillating coating for beta-particles detection. The shorter luminescence decay time allows collisions of charged particles separated by shorter intervals to be resolved and therefore provides better scintillator performance [39].

The decrease of the defect luminescence band intensity for both ZnO:Ni and ZnO:Co with the increase of the transition metal concentration in the deposition solution may be caused by the decrease of the concentration of oxygen interstitial atoms. Some of these can be bound to transition metals to form the corresponding oxide. For Ni, its oxide form was confirmed by Raman spectroscopy. Growing concentration of Ni and Co atoms in the ZnO film also causes the Zn atoms to shift from their normal positions in the semiconductor crystal lattice and leads to the formation of zinc-related defects. At a certain dopant concentration, the $Zn_i \rightarrow V_{Zn}$ transitions band appears in the luminescence spectra. The distortion of the ZnO crystal lattice with the increasing dopant concentration level was confirmed by the shift of the band corresponding to the ZnO E_2(high) vibration mode.

At high concentrations of transition atoms, both the UV NBE and defect related luminescence bands are suppressed by nonradiative recombination processes involving deep donor levels in the ZnO band gap related to Ni and Co atoms [26,40].

5. Conclusions

The ZnO doping with Ni and Co transition metals in high concentration up to degenerate levels is shown to enhance the PL and CL efficiency of the UV NBE band. The optimum result with the highest NBE band intensity was obtained after the hydrothermal deposition of ZnO:Ni and ZnO:Co films from 0.1 M $Zn(NO_3)_2$ solution containing 0.05 M of $Ni(NO_3)_2$ and $Co(NO_3)_2$. It was revealed that NBE band at room temperature is defined by free-electron/neutral acceptor irradiative recombination The NBE band at room temperature was revealed to be defined by the irradiation recombination of free electrons/neutral acceptor (eA^0). Its intensity increases with the carrier concentration in the ZnO conduction band which depends on the initial concentration of the donor doping atoms in the hydrothermal deposition solution. However, ZnO doping with a higher concentration of transitional metals is useless because nonradiative recombination suppresses irradiative processes. The ZnO:Ni and ZnO:Co films obtained also demonstrated defect luminescence bands in the visible range. In combination with near UV NBE band they cover a wide spectral range, making the films useful for optoelectronic application as a luminophore for both light emitting devices and scintillator coatings for the beta-particles detection. The low temperature hydrothermal method used also provides the opportunity to create luminescent coatings integrated on silicon substrates with electronic circuitry, for example, solid state silicon-based radiation counters.

Author statement

Eugene Chubenko: Methodology, Investigation, Writing – original draft. Mohsin Wahioh Alhamd: Conceptualization, Writing – review & editing. Vitaly Bondarenko: Writing – review & editing, Supervision.

Declaration of competing interest

The authors declare that they have no known competing financial interests or personal relationships that could have appeared to influence the work reported in this paper.

Acknowledgements

The work has been funded by the Ministry of Education of the Republic of Belarus as a part of the Belarus Government Research Program "Photonics and electronics for innovations", Grant 3.8. Authors also would like to thank D. Zhigulin from JSC "Integral" for SEM and EDX analysis and K. Yanushkevich from Scientific-Practical Materials Research Centre NAS of Belarus for XRD measurements.

References

[1] A. Kołodziejczak-Radzimska, T. Jesionowski, Zinc oxide – from synthesis to application: a review, Materials 7 (2014) 2833–2881, https://doi.org/10.3390/ma7042833.
[2] Ü. Özgür, D. Hofstetter, H. Morkoç, ZnO Devices and applications: a review of current status and future prospects, Proc. IEEE 98 (2010) 1255–1268, https://doi.org/10.1109/JPROC.2010.2044550.
[3] P.A. Rodnyi, I.V. Khodyuk, Optical and luminescence properties of zinc oxide (Review), Opt Spectrosc. 111 (2011) 776–785, https://doi.org/10.1134/S0030400X11120216.
[4] Ü. Özgür, YaI. Alivov, C. Liu, A. Teke, M.A. Reshchikov, S. Doğan, V. Avrutin, S.-J. Cho, H. Morkoç, A comprehensive review of ZnO materials and devices, J. Appl. Phys. 98 (2005), 041301, https://doi.org/10.1063/1.1992666.
[5] D.M. Bagnall, Y.F. Chen, Z. Zhu, T. Yao, High temperature excitonic stimulated emission from ZnO epitaxial layers, Appl. Phys. Lett. 73 (1998) 1038–1040, https://doi.org/10.1063/1.122077.
[6] B.K. Meyer, H. Alves, D.M. Hofmann, W. Kriegseis, D. Forster, F. Bertram, J. Christen, A. Hoffmann, M. Straßburg, M. Dworzak, U. Haboeck, A.V. Rodina, Bound exciton and donor-acceptor pair recombinations in ZnO, Phys. Status Solidi B 241 (2004) 231–260, https://doi.org/10.1002/pssb.200301962.
[7] P.J. Simpson, R. Tjossem, A.W. Hunt, K.G. Lynn, V. Munné, Superfast timing performance from ZnO scintillators, Nucl. Instrum. Methods Phys. Res., Sect. A 505 (2003) 82–84, https://doi.org/10.1016/S0168-9002(03)01025-8.
[8] C. Dujardin, E. Auffray, E. Bourret-Courchesne, P. Dorenbos, P. Lecoq, M. Nikl, A. N. Vasil'ev, A. Yoshikawa, R.-Y. Zhu, Needs, trends, and advances in inorganic scintillators, IEEE Trans. Nucl. Sci. 65 (2018) 1977, https://doi.org/10.1109/TNS.2018.2840160, 1997.
[9] M. Koshimizu, T. Yanagida, R. Kamishima, Y. Fujimoto, K. Asai, Scintillation properties and α-ray detection capabilities of thin-film plastic scintillators, Sensor. Mater. 31 (2019) 1233–1239, https://doi.org/10.18494/SAM.2019.2182.
[10] E.D. Bourret-Courchesne, S.E. Derenzo, M.J. Weber, Development of ZnO:Ga as an ultra-fast scintillators, Nucl. Instrum. Methods Phys. Res., Sect. A 601 (2009) 358–363, https://doi.org/10.1016/j.nima.2008.12.206.
[11] Q. Li, X. Liu, M. Gu, Y. Hu, F. Li, S. Liu, Q. Wu, Z. Sun, J. Zhang, S. Huang, Z. Zhang, J. Zhao, Development of ZnO-based nanorod arrays as scintillator layer for ultrafast and high-spatialresolution X-ray imaging system, Opt Express 26 (2018) 31290–31298, https://doi.org/10.1364/OE.26.031290.
[12] J.S. Neal, D.M. DeVito, B.L. Armstrong, M. Hong, B. Kesanli, X. Yang, N.C. Giles, J. Y. Howe, J.O. Ramey, D.J. Wisniewski, M. Wisniewska, Z.A. Munir, L.A. Boatner, Investigation of ZnO-based polycrystalline ceramic scintillators for use as α-particle detectors, IEEE Trans. Nucl. Sci. 56 (2009) 892–898, https://doi.org/10.1109/TNS.2008.2004702.
[13] P.A. Rodnyi, K.A. Chernenko, E.I. Gorokhova, S.S. Kozlovskii, V.M. Khanin, I. V. Khodyuk, Novel scintillation material – ZnO transparent ceramics, IEEE Trans. Nucl. Sci. 59 (2012) 2152–2155, https://doi.org/10.1109/TNS.2012.2189896.
[14] E.I. Gorokhova, G.V. Anan'eva, V.A. Demidenko, P.A. Rodny, I.V. Khodyuk, E. D. Bourret-Courchesne, Optical, luminescence, and scintillation properties of ZnO and ZnO:Ga ceramics, J. Opt. Technol. 75 (2008) 741–746, https://doi.org/10.1364/JOT.75.000741.
[15] X. Wen, Q. Zhang, Z. Shao, Magnetron sputtering for ZnO:Ga scintillation film production and its application research status in nuclear detection, Crystals 9 (2019) 263, https://doi.org/10.3390/cryst9050263.
[16] L.-N. Tong, T. Cheng, H.-B. Han, J.-L. Hu, X.-M. He, Y. Tong, C.M. Schneider, Photoluminescence studies on structural defects and room temperature ferromagnetism in Ni and Ni–H doped ZnO nanoparticles, J. Appl. Phys. 108 (2010), 023906, https://doi.org/10.1063/1.3460644.
[17] S. Taguchi, T. Tayagaki, Y. Kanemitsu, Luminescence and magnetic properties of Co doped ZnO nanocrystals, IOP Conf. Ser. Mater. Sci. Eng. 6 (2009), 012029, https://doi.org/10.1088/1757-899X/6/1/012029.
[18] P. Zaumseil, High-resolution characterization of the forbidden Si 200 and Si 222 reflections, J. Appl. Crystallogr. 48 (2015) 528–532, https://doi.org/10.1107/S1600576715004732.
[19] I. Iatsunskyi, S. Jurga, V. Smyntyna, M. Pavlenko, V. Myndrul, A. Zaleska, Raman spectroscopy of nanostructured silicon fabricated by metal-assisted chemical etching, Proc. SPIE 9132 (2014) 913217, https://doi.org/10.1117/12.2051489.
[20] A. Zaoui, W. Sekkal, Pressure-induced softening of shear modes in wurtzite ZnO: a theoretical study, Phys. Rev. B 66 (2002) 174106, https://doi.org/10.1103/PhysRevB.66.174106.
[21] N. Ashkenov, B.N. Mbenkum, C. Bundesmann, V. Riede, M. Lorenz, D. Spemann, E. M. Kaidashev, A. Kasic, M. Schubert, M. Grundmann, Infrared dielectric functions and phonon modes of high-quality ZnO films, J. Appl. Phys. 93 (2003) 126–133, https://doi.org/10.1063/1.1526935.

[22] G.A. Babu, G. Ravi, T. Mahalingam, M. Kumaresavanji, Y. Hayakawa, Influence of microwave power on the preparation of NiO nanoflakes for enhanced magnetic and supercapacitor applications, Dalton Trans. 44 (2015) 4485–4497, https://doi.org/10.1039/C4DT03483J.
[23] D.S. Hall, D.J. Lockwood, C. Bock, B.R. MacDougall, Nickel hydroxides and related materials: a review of their structures, synthesis and properties, Proc. R. Soc. A. 471 (2014) 20140792, https://doi.org/10.1098/rspa.2014.0792.
[24] C.H. Ahn, Y.Y. Kim, D.C. Kim, S.K. Mohanta, H.K. Cho, A comparative analysis of deep level emission in ZnO layers deposited by various methods, J. Appl. Phys. 105 (2009), 013502, https://doi.org/10.1063/1.3054175.
[25] S. Vempati, J. Mitra, P. Dawson, One-step synthesis of ZnO nanosheets: a blue-white fluorophore, Nanoscale Res. Lett. 7 (2012) 470, https://doi.org/10.1186/1556-276X-7-470.
[26] J. Xu, S. Shi, L. Li, X. Zhang, Y. Wang, Q. Shi, S. Li, H. Wang, Luminescence properties of cobalt-doped ZnO films prepared by sol-gel method, J. Electron. Mater. 42 (2013) 3438–3444, https://doi.org/10.1007/s11664-013-2719-4.
[27] S.K. Mandal, A.K. Das, T.K. Nath, D. Karmakar, Temperature dependence of solubility limits of transition metals (Co, Mn, Fe, and Ni) in ZnO nanoparticles, Appl. Phys. Lett. 89 (2006) 144105, https://doi.org/10.1063/1.2360176.
[28] C.A. Arguello, D.L. Rousseau, S.P.S. Porto, First-order Raman effect in wurtzite-type crystals, Phys. Rev. 181 (1969) 1351–1363, https://doi.org/10.1103/PhysRev.181.1351.
[29] C. Bundesmann, N. Ashkenov, M. Schubert, D. Spemann, T. Butz, E.M. Kaidashev, M. Lorenz, M. Grundmann, Raman scattering in ZnO thin films doped with Fe, Sb, Al, Ga, and Li, Appl. Phys. Lett. 83 (2003) 1974–1976, https://doi.org/10.1063/1.1609251.
[30] S.C. Das, R.J. Green, J. Podder, T.Z. Regier, G.S. Chang, A. Moewes, Band gap tuning in ZnO through Ni doping via spray pyrolysis, J. Phys. Chem. C 117 (2013) 12745–12753, https://doi.org/10.1021/jp3126329.
[31] R. Elilarassi, G. Chandrasekaran, Synthesis, structural and optical characterization of Ni-doped ZnO nanoparticles, J. Mater. Sci. Mater. Electron. 22 (2011) 751–756, https://doi.org/10.1007/s10854-010-0206-8.
[32] J. Hugel, C. Carabatos, Band structure and optical properties of NiO. I. Band structure calculations, J. Phys. C Solid State Phys. 16 (1983) 6713–6721, https://doi.org/10.1088/0022-3719/16/35/005.
[33] N.M. Hosny, Synthesis, characterization and optical band gap of NiO nanoparticles derived from anthranilic acid precursors via a thermal decomposition route, Polyhedron 30 (2011) 470–476, https://doi.org/10.1016/j.poly.2010.11.020.
[34] L. Vegard, Die konstitution der mischkristalle und die raumfüllung der atome, Z. Physik 5 (1921) 17–26, https://doi.org/10.1007/BF01349680.
[35] A. Walsh, J.L.F. Da Silva, S.-H. Wei, Origins of band-gap renormalization in degenerately doped semiconductors, Phys. Rev. B 78 (2008), 075211, https://doi.org/10.1103/PhysRevB.78.075211.
[36] L.-N. Tong, T. Cheng, H.-B. Han, J.-L. Hu, X.-M. He, Y. Tong, C.M. Schneider, Photoluminescence studies on structural defects and room temperature ferromagnetism in Ni and Ni–H doped ZnO nanoparticles, J. Appl. Phys. 108 (2010), 023906, https://doi.org/10.1063/1.3460644.
[37] H.S. Kang, G.H. Kim, S.H. Lim, H.W. Chang, J.H. Kim, S.Y. Lee, Relationship between ultraviolet emission and electron concentration of ZnO thin films, Thin Solid Films 516 (2008) 3147–3151, https://doi.org/10.1016/j.tsf.2007.08.084.
[38] B.P. Zhang, N.T. Binh, Y. Segawa, Y. Kashiwaba, K. Haga, Photoluminescence study of ZnO nanorods epitaxially grown on sapphire (1120) substrates, Appl. Phys. Lett. 84 (2004) 586–588, https://doi.org/10.1063/1.1642755.
[39] Q. Li, X. Liu, M. Gu, Y. Hu, F. Li, S. Liu, Q. Wu, Z. Sun, J. Zhang, S. Huang, Z. Zhang, J. Zhao, Development of ZnO-based nanorod arrays as scintillator layer for ultrafast and high-spatialresolution X-ray imaging system, Opt Express 26 (2018) 31290–31298, https://doi.org/10.1364/OE.26.031290.
[40] M. Schmidt, K. Brachwitz, F. Schmidt, M. Ellguth, H. von Wenckstern, R. Pickenhain, M. Grundmann, G. Brauer, W. Skorupa, Nickel-related defects in ZnO – a deep-level transient spectroscopy and photo-capacitance study, Phys. Status Solidi B 248 (2011) 1949–1955, https://doi.org/10.1002/pssb.201046634.